A PARAMETRIC STUDY OF HARD TISSUE INJURY PREDICTION USING FINITE ELEMENTS: CONSIDERATION OF GEOMETRIC COMPLEXITY, SUB-FAILURE MATERIAL PROPERTIES, CT-THRESHOLDING, AND ELEMENT CHARACTERISTICS

Carlos Arregui-Dalmases, Eduardo Del Pozo
European Center for Injury Prevention, Universidad de Navarra

Sonia Duprey, Francisco J. Lopez-Valdes, Anthony Lau, Damien Subit, Richard Kent
Center for Applied Biomechanics, University of Virginia

ABSTRACT

This study quantifies the sensitivity of finite element-predicted fracture in the clavicle to several parameters. Clavicles were harvested from 14 donors (age range 14-56 years). Quasistatic axial compression tests were performed using a custom rig designed to replicate *in situ* boundary conditions. Prior to testing, high-resolution computed tomography (CT) scans were taken of each clavicle. From those images, finite element models were constructed. Factors varied parametrically included the density used to threshold cortical bone in the CT scans, the presence of trabecular bone, the mesh density, Young's modulus, the maximum stress, and the element type (shell vs. solid, triangular vs. quadrilateral surface elements). The experiments revealed significant variability in the peak force (2.41±0.72 kN) and displacement to peak force (4.9±1.1 mm), with age ($p<0.05$) and with some geometrical traits of the specimens. In the FE models, the failure force and location were moderately dependent upon the Young's modulus. The fracture force was highly sensitive to the Maximun stress (80-110 MPa). Neither fracture location nor force was strongly dependent on mesh density. Both the fracture location and force were strongly dependent upon the threshold density used to define the thickness of the cortical shell.

Keywords: Finite element modeling, fracture prediction, clavicle, side impact, sensitivity study

WHOLE-BODY FINITE ELEMENT (FE) models play an increasingly important role in vehicle safety system design for injury mitigation, but the validation of these models remains very coarse. The accurate representation of complex geometries and the ability to calculate material-level mechanical responses are the primary advantages of FE, yet injury-level validation is typically not attempted in whole-body FE models, nor is validation at the material stress-strain level. With a few exceptions (e.g. Iwamoto et al. 2005), gross structural behaviors measured experimentally are considered the gold standard for response validation at both the whole-body and the component level (e.g., Kimpara et al. 2005, Ruan et al. 2003, 2006). Bony fracture, not to mention visceral and other types of trauma having even more complex mechanisms, has not been robustly validated in any FE model of the whole-body or of any significant whole-body sub-structure. This is at least partially due to the computational time required to simulate whole-body or body-component behaviors. Even highly focused FE models of small bone samples, with sub-mm elements and models of individual trabeculae, may not be sufficient for modeling the complex crack propagation and failure mechanisms that occur in bone unless computationally expensive algorithms for modeling fracture mechanics of anisotropic composites are incorporated (e.g., Nalla et al. 2005a, b). As computational power increases, so does the precision with which bony geometry can be represented in a whole-body FE model, but the level of detail required to model actual mechanisms of crack propagation and failure in bone will likely not be feasible for decades in a model of that size. Thus, there is a need for pragmatic assessments of techniques for defining and simplifying methods for predicting bone fracture with a relatively coarse FE model. Past researchers have studied this issue, including several papers assessing fracture prediction in the femur during locomotion and as a result of a fall (Ford et al. 1996, Keyak et al. 1998, Keyak and Rossi 2000, Lotz et al. 1991a, b). These studies have employed existing failure theories based on stress or strain to predict the timing of location of bony fracture, recognizing

that there is no stress- or strain-based failure theorem developed and validated specifically for the prediction of bony fracture. Thus, failure theories such as Mohr, Coulomb-Mohr, Tresca, Hoffman, maximum values of various components of stress or strain tensors, and distortion energy have been assessed in FE models for their phenomenological ability to replicate experimental observations. The studies listed above did not, however, assess the significance of geometric variation in the particular bones being studied, nor the methods employed in the development of the finite element mesh from medical images of the bones and the type of element used. The findings of Charpail et al. (2005) and Charpail (2006) suggest that variations in the geometry of the bone may have a much larger effect on the location and timing of fracture than variations in the particular failure theory used. Furthermore, since the transition from cortical to trabecular bone is not discrete, the particular thresholding approach taken when defining the volume of cortical bone in CT scans may also be a dominant factor in modeling the failure characteristics of a bone (e.g., Boyd and Muller 2005). Even CT parameters such as peak voltage, slice thickness and in-plane resolution, and the particular machine used for the scan have been shown to significantly influence the thresholding of cortical bone and the accuracy of finite element calculations (Camacho et al. 1997, Ladd and Kinney 1998, Pettersen et al. 2006).

It is clear from the above review that a large number of factors contribute to the outputs generated by an FE bone model developed from medical images. In fact, any FE model developed in this fashion will have so many independent parameters affecting the output that no set can be said to be uniquely "correct". In other words, relative to the experimental data typically available for benchmarking, the model parameters will be grossly under-determined. This fact calls into question the typical practice of "validating" a model by tuning selected parameters (usually material model coefficients) such that a set of experimental data are reproduced to some level of precision. This study is an attempt to quantify the sensitivity of FE-predicted sub-failure behavior and fracture location and timing to several potentially important parameters that have previously not been assessed as a group, including material properties, failure threshold, thresholding assumptions, and element type and density. One hypothesis of this study is that geometric factors, such as curvature and cortical thickness, are dominant for predicting fracture force and location. The clavicle was chosen for study since it is relatively understudied in the literature, it has a complex geometry that is highly variable among subjects, it is easily harvested and of convenient size for both medical imaging and testing, and it is an important load path in lateral impacts.

METHODS

Quasistatic axial compression tests were performed using a custom rig designed to create boundary conditions that were considered to be a reasonable representation of the clavicle extremities *in situ* (see Compigne et al. 2000), but sufficiently simple and defined to facilitate accurate modeling. Prior to testing, high-resolution computed tomography (CT) scans were taken of each clavicle. From those images, finite-element models were constructed of each clavicle, which were then used in a parametric study to assess the relative importance of various factors for predicting the location and timing of fracture. The methods for each of these aspects of the research are described in detail below.

COMPRESSION TESTS: One clavicle was harvested from each of 14 donors (age range 14-56 years,3 female,). The clavicles were provided by the Department of Anatomy of the Medical University of Navarra, the Pathological Anatomy Service at the Clinica Universitaria de Navarra (CUN) and the Tissue Donor Program of Hospital Virgen del Camino, Comunidad Foral de Navarra. The soft tissue adjacent to the bone was carefully removed and the bones were stored at -20ºC in individual bags. The storage period varied from 1 week to 10 months. One day prior to the test, the bones were thawed at room temperature. During thawing and prior to preparation for testing the bones were wrapped in saline-soaked gauze.

Table 1. Specimen and test information and selected results (all tests performed at 0.63 mm/s).

Subject	Age	Gender	Aspect	Max. Force (N)	Disp. at Max. Force (mm)	Fracture Force† (N)	Disp. at Fracture (mm, % of S_1)	Stiffness* (N/mm)
ECIP 01§	47	M	R	2478	4.0	2475	3.2 mm, 2.2%	835.1
ECIP 03	49	M	L	2692	5.1	1362	9.5 mm, 5.8%	767.5
ECIP 04	54	M	L	3324	6.6	3135	6.7 mm, 4.0%	769.8
ECIP 05	55	M	L	2235	5.1	2067	6.8 mm, 4.0%	541.4
ECIP 06	56	M	L	3310	4.0	3310	4.0 mm, 2.5%	1405.0
ECIP 07	56	M	L	2167	6.8	2057	7.6 mm, 5.1%	680.8
ECIP 08	23	M	R	2966	4.6	1495	10.5 mm, 7.2%	1065.5
ECIP 09	37	M	R	1672	5.1	1308	12.4 mm, 7.7%	435.7
ECIP 10	14	F	L	1207	3.2	624	9.1 mm, 6.9%	532.2
ECIP 11	43	F	R	2359	4.6	1016	12.3 mm, 8.2%	818.2
ECIP 12§	46	M	R	2178	6.4	1926	12.4 mm, 8.3%	957.7
ECIP 13	46	F	L	1570	3.7	1165	8.2 mm, 5.6%	588.2
ECIP 14§	42	M	R	1878	4.5	1729	6.0 mm, 3.7%	613.7
ECIP 15	56	M	R	3665	4.7	3110	7.4 mm, 4.7%	997.5
Avg. ± s.d.	44.6±12.7			2407±720	4.9±1.1	1912±839	8.3±2.9 mm, 5.4±2.0%	786.3±258.2

†Fracture force defined as first abrupt drop in force (see circled points in Fig. 4)
*Linear regression to force-displacement up to maximum force.
§Possibly artifactual fracture, data excluded from further analysis (see Fig. 6).

Using a methodology similar to that described by Duprey (2008), both ends of the clavicles were potted within aluminum cups using a two-part self-curing urethane compound (Product 891, Goldenwest Mfg., Inc., Cedar Ridge, CA, USA). The test samples were potted within a cylindrical template to ensure a consistent axial orientation of the loading. The potted test sample was then mounted into a custom rig that was driven by a universal material test machine (Instron Model 4500; Norwood, MA, USA). A clavicle-fixed coordinate system was defined as shown in Figure 1. The boundary condition at the acromial (lateral) extremity of the clavicle allowed no rotation and displacement only in the Z direction. The boundary condition at the sternal (medial) end allowed no displacement, and rotation only about the X (approximately the body's longitudinal) axis.

The test fixture was mounted within the test machine such that the clavicle was in a vertical orientation with the acromial end at the cross-head. Testing was initiated with an applied displacement of the cross-head, which generated a compressive load on the clavicle. Instrumentation included a uniaxial (tension-compression) load cell (INSTRON 2518-804, Norwood, MA, USA) mounted at the acromial end of the clavicle, and a 6-axis load cell (MC3A-6-1000, Advanced Mechanical Technology Inc, Watertown, MA, USA) and rotary potentiometer mounted at the sternal end. The rotary potentiometer measured rotation about the X axis (the lone degree of freedom at the sternal extremity). Data were collected at 2000 Hz using a National Instruments Model NI cDAQ-9172 data acquisition system (modules NI9237 and NI 9215, National Instruments Corporation, Austin, TX, USA) and filtered according to recommended practices. Tests were further documented using digital photography and videography.

The peak force was defined as the maximum value of F_Z, and the fracture force was defined as the magnitude of F_Z immediately before the first abrupt drop. The relationships between force and displacement values, geometric characteristics, and traits of the donor (age, gender) were assessed using correlation analysis, linear regressions, paired t-tests (for data with a normal distribution), and Wilcoxon tests (for non-parametric data). The normality of the data was checked through 3 different tests (Shapiro-Wilk W test, Skewness/Kurtosis test, Shapiro-Francia W' test). Statistical analyses were performed with Stata 9.0 (Stata, College Station, Texas).

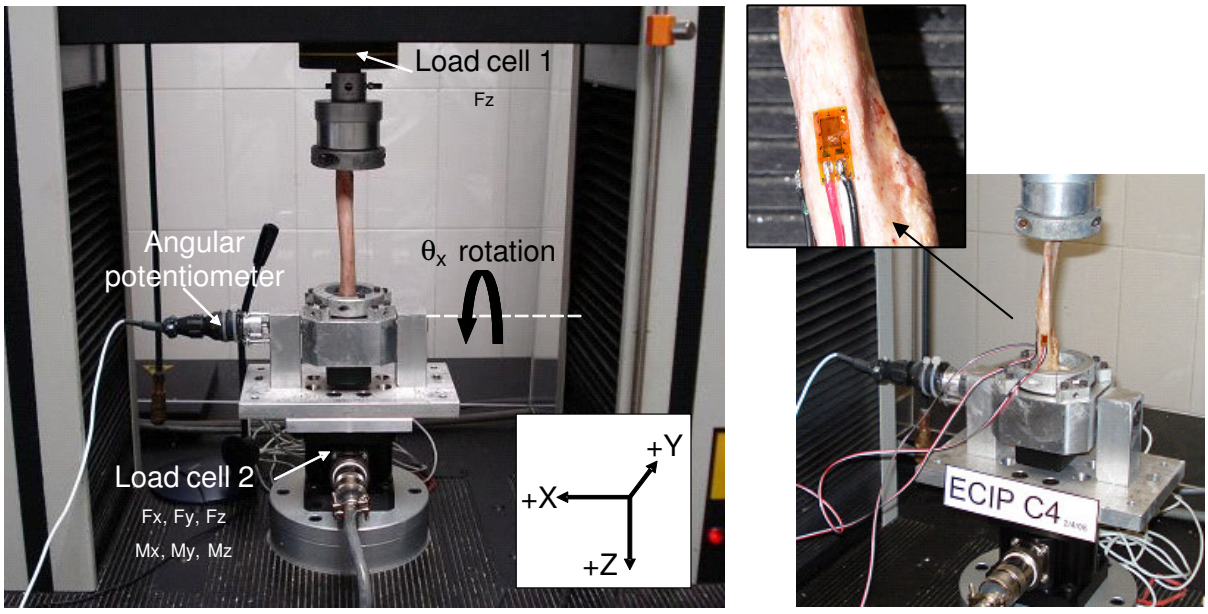

Fig. 1 - Test set-up and reference system.

COMPUTATIONAL MODELING AND PARAMETRIC STUDY DESIGN: Ten finite element models were created for each of the 14 tested clavicles, and axial compression loading of each clavicle model was simulated (Figure 2). Thus, a total of 140 simulations was performed; RADIOSS (Altair, Troy, MI, USA) was used as the FE model solver. The input crosshead displacement measured in the experiments was used as the input to the FE simulation. Bone was modeled as elastic-perfectly plastic (reduced form of RADIOSS material Johnson-Cook). The Poisson's ratio was set to 0.3 for cortical bone and to 0.4 for trabecular bone. Bone fracture was defined as the point in time when both the first principle strain and the first principle stress exceeded the defined maximum stress and maximum strain values. Maximum stress was varied parametrically (Table 2), but maximum strain was defined as 0.015 for cortical bone and 0.9 for trabecular bone and was not varied. The densities of cortical (1.8 kg/L) and trabecular (1.0 kg/L) bone were likewise defined nominally based on values from the literature.

CT data for all clavicles were collected at CUN using a slice thickness of 0.6 mm and an in-plane 512x512 matrix resolution of 6.051 pixels/mm (Somaton Sensation 64, Siemens, New York). The external geometry and the thickness of the cortical shell were determined from the CT scans, where the threshold for cortical bone was defined using three different, but all reasonable, HU values. The baseline HU necessarily varied slightly among clavicles, and was identified qualitatively as the value giving the most reasonable visual representation of the cortical shell. Since the definition of the cortical shell boundary in CT images is somewhat subjective, HU values defined as "baseline^{minus}" and "baseline^{plus}" were defined for consideration in the parametric study. These were HU values that were less than and greater than the baseline, yet still yielded a reasonable geometric representation of the cortical bone. In cases where the trabecular bone was modeled, the entire volume within the cortical contours was defined as trabecular bone regardless of HU.

Several shape features of the clavicles were measured using the CT data following the methodology of Andermahr et al. (2007). These features included diameters at different sections of the bone as well as depths and radii of the two curvatures of the clavicle (Fig. 3). Automatic mesh generation methods were employed within the software packages Blender (Blender Foundation, Amsterdam) and Hypermesh (Altair, Troy, MI, USA). Three element types were considered: triangular shell elements, quadrangular shell elements, and tetrahedral solid elements. The thickness of the cortical part was defined as a mean value from the CT scans. Two levels of mesh coarseness

were created, and two values of Young's modulus and maximum stress for the cortical bone were assessed.

The applied force and input displacement at the point of "bone fracture" as defined above, as well as the location of the "fractured" elements were identified from the FE solver output.

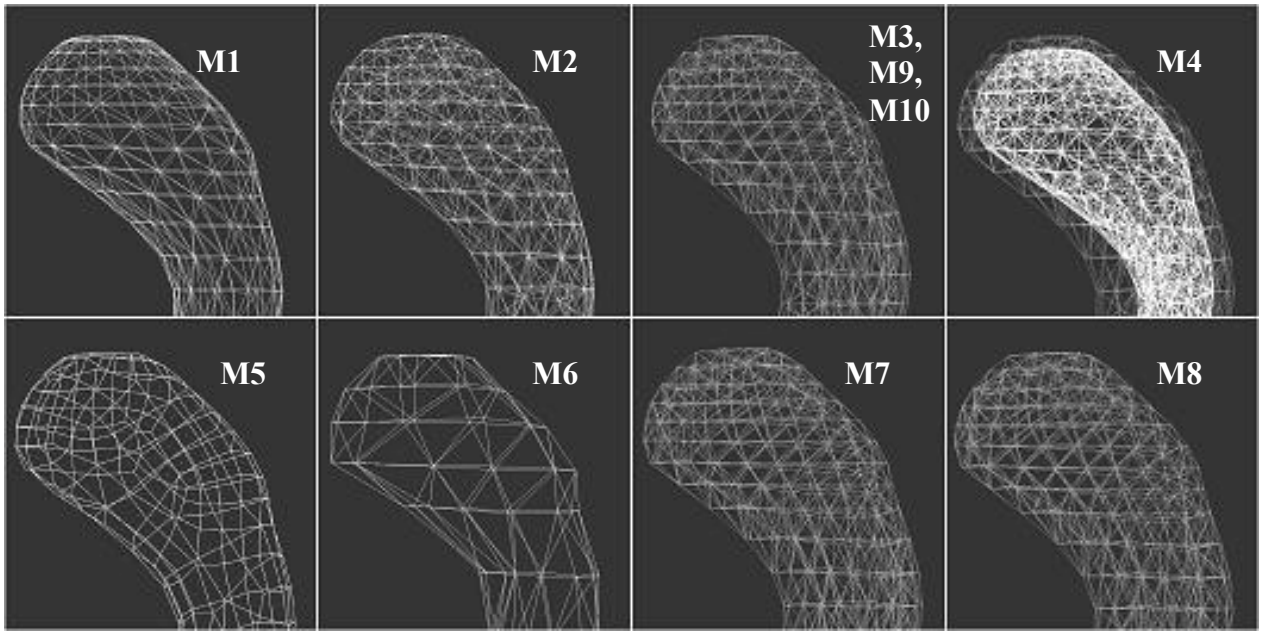

Fig. 2 - Ten different FE models (M1-M10) created for each clavicle.

Table 2. Summary of the simulation models used in the parametric study.

Model	Material	Young's modulus, E_Y (GPa)	Max. stress, T_{max} (MPa)	Threshold (HU)	Element Type*	Element edge length (mm)
1	Cortical bone	1.6	110	Baseline	1	~2
	Trabecular bone			Not modeled		
2	Cortical bone	1.6	110	Baseline	1	~2
	Trabecular bone	0.5	4	All	3	~2
3	Cortical bone	1.6	110	Baseline	3	~2
	Trabecular bone			Not modeled		
4	Cortical bone	1.6	110	Baseline	3	~2
	Trabecular bone	0.5	4	All	3	~2
5	Cortical bone	1.6	110	Baseline	2	~2
	Trabecular bone			Not modeled		
6	Cortical bone	1.6	110	Baseline	1	~5
	Trabecular bone			Not modeled		
7	Cortical bone	1.6	110	$Baseline^{minus}$	3	~2
	Trabecular bone			Not modeled		
8	Cortical bone	1.6	110	$Baseline^{plus}$	3	~2
	Trabecular bone			Not modeled		
9	Cortical bone	1.2	110	Baseline	3	~2
	Trabecular bone			Not modeled		
10	Cortical bone	1.6	80	Baseline	3	~2
	Trabecular bone			Not modeled		

*1 – Triangular shell elements; 2 – Quadrangular shell elements; 3 – Tetrahedral solid elements

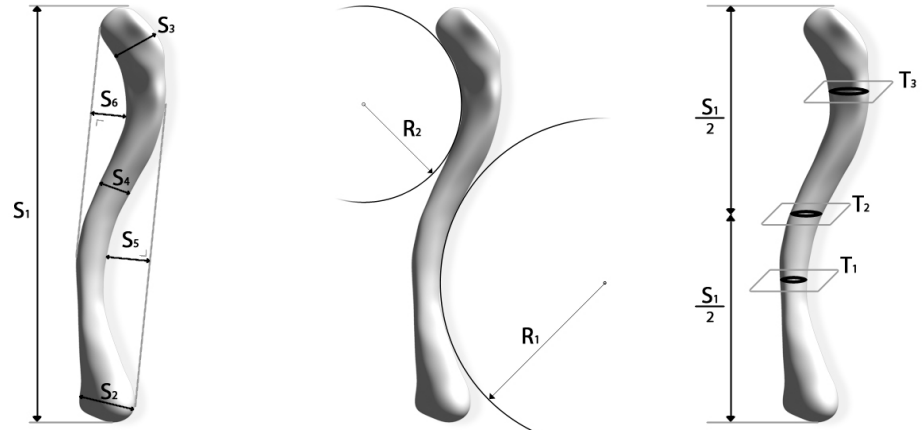

Fig. 3 - Parameters used for the description of the geometry of the clavicle.

RESULTS

COMPRESSION TESTS: Tests were completed successfully on all 14 clavicles. The compression (F_Z) force and cross-head displacement were the primary data of interest. This force increased approximately linearly with displacement up to between 1 and 4 mm (Fig. 4) before exhibiting a concave-down characteristic that was smooth in most cases, and finally an abrupt decrease that was defined as the point of fracture. However this characteristic was not universal, some clavicles exhibiting a more gradual fracture onset (see circles in Fig. 4). The peak force varied substantially, from 1.2 kN in the 14-year-old female specimen to 3.7 kN in a 56-year-old male (Table 1). The displacement at peak force ranged from 3.2 mm to 6.8 mm (mean 4.9 mm). Interestingly, there appeared to be no obvious relationship between the peak force and the fracture force, with the post-peak behavior varying across specimens. The fracture force ranged from 43% to 100% of the peak force, with the magnitude ranging from 624 N (again, in the 14-year-old) to 3.3 kN in a 56-year-old male. Likewise, the displacement at fracture varied substantially, from 4.0 mm (2.5% of initial length) to 12.4 mm (8.3%). The linear stiffness prior to the peak force varied from 436 N/mm in a 37-year-old to 1.4 kN/mm in a 56-year-old.

The other forces measured at the sternal end of the specimens were generally low compared to F_Z (see representative plots in Figure 5), with the laterally directed forces rarely exceeding 150 N.

The means and variance in the geometric features of the tested clavicles (Table 3) were consistent with those measured in other studies (Andermahr et al. 2007, Duprey 2007). Likewise, the fracture location most often observed in this study was consistent with those earlier studies, with most fractures occurring in the middle third and biased toward the sternal end (Fig. 6). Three of the fractures occurred near the sternal fixation. These were considered artifactual and the data from those specimens were not considered in the analysis.

CORRELATION ANALYSIS OF EXPERIMENTAL DATA: Age was positively correlated ($R^2 \geq 0.5$, see bold in Table 4) with the maximum force and the fracture force, and negatively correlated with the percent displacement at fracture. The signs of these correlations differ from most cadaver-based studies in the injury biomechanics literature, and reflects the fact that the age distribution of the subjects studied here is young. Instead of reflecting, as most cadaver-based studies do, the effects of senescence, these data appear to illustrate the development, increase in force tolerance, and decrease in failure strain that occur between age 14 and adulthood.

The geometric characteristics of the clavicles were also correlated with failure tolerance, with the fracture force being correlated with S_3 and, most strongly, with S_4. The thickness of the cortical shell and the length of the clavicle had correlation coefficients close to 0.5 for fracture force, as did the depth of the medial curvature, S_5.

COMPUTATIONAL MODELING AND PARAMETRIC STUDY: Each of the ten models generated a different value of peak force and peak displacement (displacement at "fracture") for each clavicle (Table 5, Table 6). Averaged over all of the clavicles, model 8 (M8) generated the highest peak force (4.1 kN). This was the model with the lowest threshold for cortical bone and thus more material defined as cortical bone in the model and a thicker cortical layer representation in the model. In contrast, M7, which was identical to M8 except for the HU level used to define the cortical layer thickness, generated a significantly lower peak force (3.5 kN, Table 7). The model M10 generates the lowest mean peak force (3.0 kN), this model had a maximum stress value of 80 MPa. In contrast, M3, which had identical parameters with a maximun stress of 110 MPa generated a mean peak force of 3.9 kN. The other material parameter that was studied, Young's modulus, did not have a large effect over the range evaluated here, with a reduction from 1.6 GPa to 1.2 GPa resulting in less than a 5% reduction in mean peak force (M9 vs. M3). The addition of trabecular bone did not have a large effect (M1 vs. M2, M3 vs. M4), though the peak force and displacement both increased slightly (< 5% on average). The element type (M1 vs. M3 vs. M5) also affected the peak force and displacement, with the solid element model (M3) generating greater force and displacement than either of the shell element models. The quadrangular shell elements generated slightly less force and displacement than the triangular shell elements. An approximately two-fold increase in element size (M1 vs. M6) resulted in a slight increase in peak force (~8%) and in "fracture" displacement (~3%).

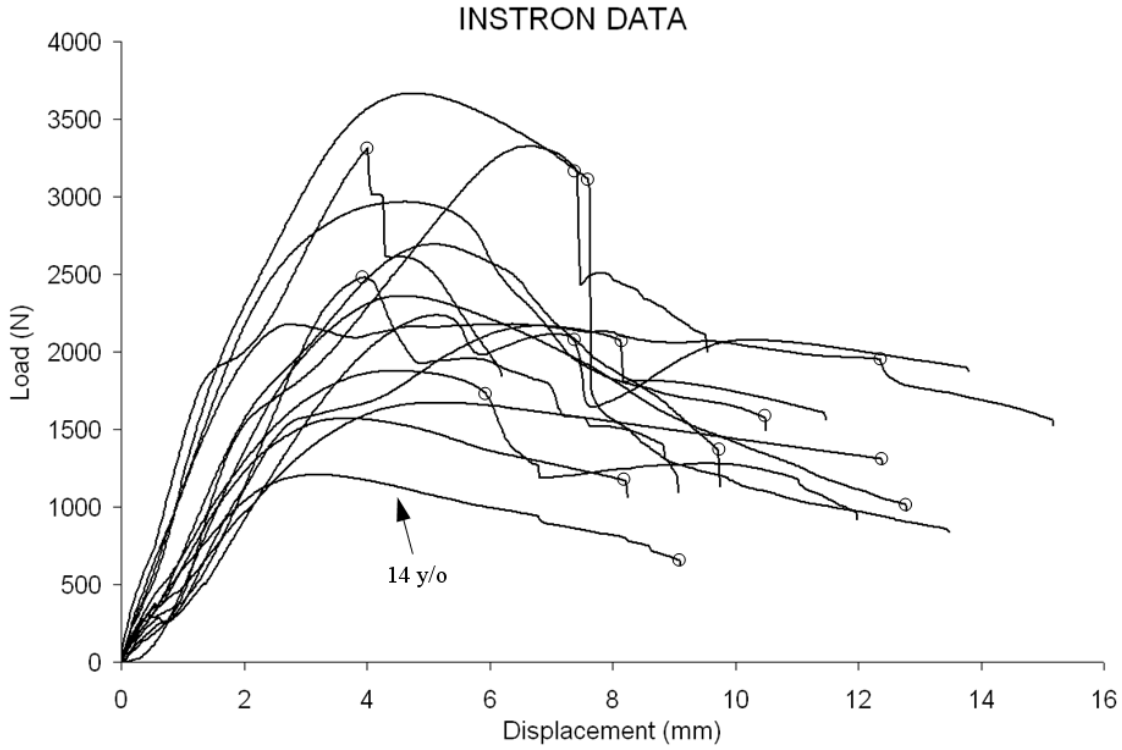

Fig. 4 - Load-time curves of the experimental tests (defined failure point circled).

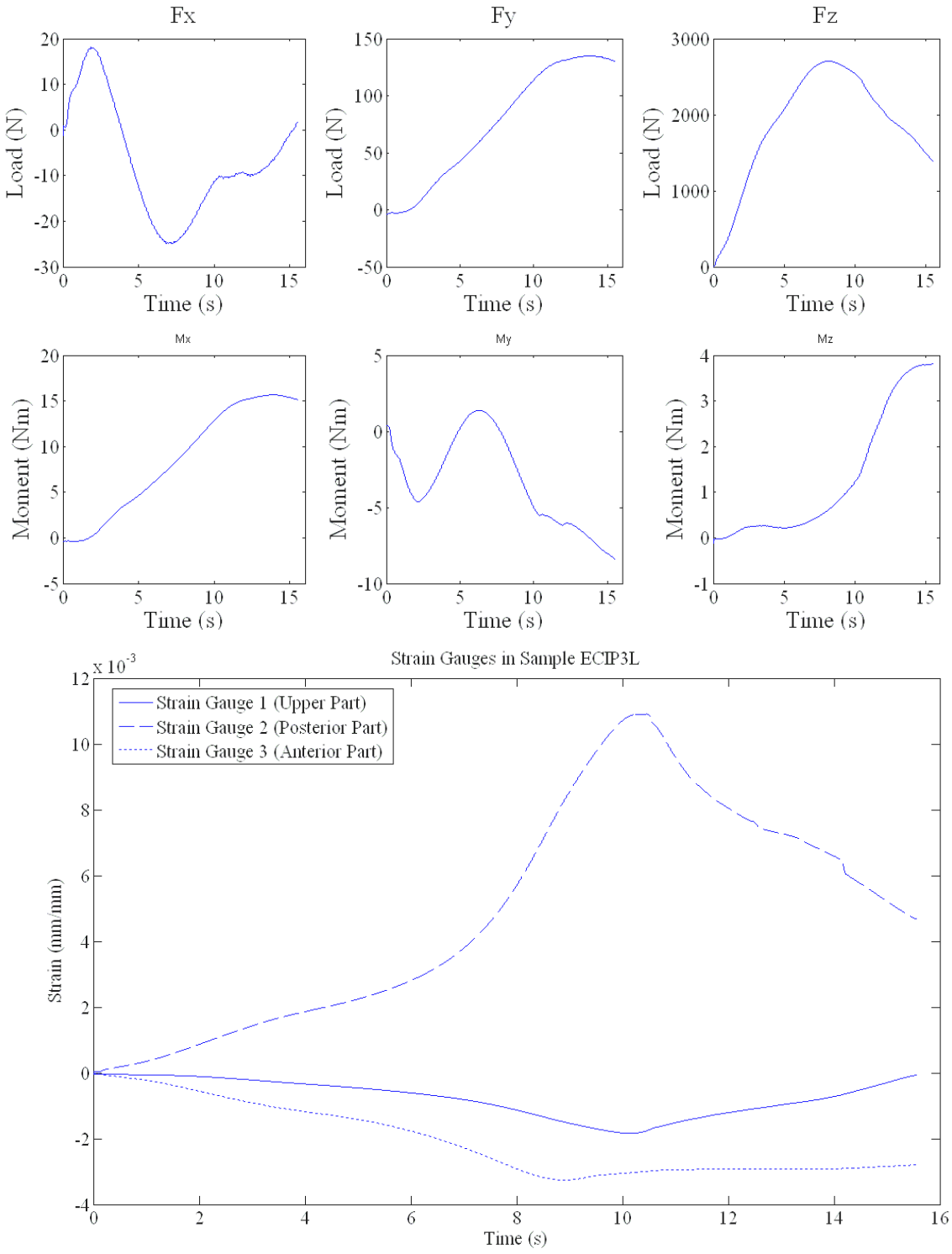

Fig. 5 Strain gauges measurements, Forces and Moments measured at the sternal end for specimen ECIP3 (typical).

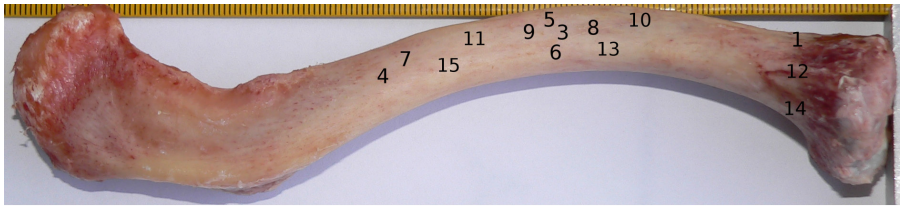

Fig. 6 Locations of the fractures in each of the specimens, shown on a generic clavicle.

Table 3. Geometrical description of the specimens (cm, see Fig. 3).

Subject	S_1	S_2	S_3	S_4	S_5	S_6	R_1	R_2	T_1	T_2	T_3
ECIP 01	14.48	2.29	2.62	1.55	1.68	1.27	5.72	2.42	0.14	0.23	0.15
ECIP 03	16.40	2.59	2.29	1.23	1.53	1.42	8.72	2.85	0.25	0.32	0.33
ECIP 04	16.83	2.52	2.62	1.38	2.66	1.56	6.46	2.51	0.35	0.44	0.28
ECIP 05	16.85	2.70	2.49	1.27	2.71	1.46	7.15	2.44	0.34	0.39	0.27
ECIP 06	15.94	2.44	2.55	1.54	2.10	1.51	6.72	2.24	0.42	0.42	0.41
ECIP 07	14.83	2.40	2.23	1.39	1.90	1.11	6.53	1.80	0.23	0.37	0.23
ECIP 08	14.61	2.31	2.40	1.34	1.61	1.65	7.12	1.82	0.21	0.22	0.20
ECIP 09	16.05	2.62	2.41	1.46	2.30	1.56	6.41	3.85	0.30	0.30	0.16
ECIP 10	13.21	2.23	2.25	1.17	1.46	0.73	5.80	1.92	0.21	0.33	0.36
ECIP 11	15.09	2.40	2.30	1.20	1.37	1.53	6.30	2.55	0.20	0.28	0.33
ECIP 12	14.90	3.04	2.82	1.70	2.17	0.74	6.65	3.91	0.20	0.26	0.16
ECIP 13	14.72	2.18	2.00	1.26	1.77	1.04	6.84	3.23	0.19	0.28	0.26
ECIP 14	16.20	2.79	2.01	1.29	1.08	1.55	10.42	3.92	0.19	0.29	0.29
ECIP 15	15.64	2.93	2.45	1.75	1.62	0.89	8.24	4.32	0.21	0.26	0.24
Mean	15.41	2.53	2.39	1.40	1.85	1.29	7.08	2.84	0.24	0.31	0.26
St. Dev.	1.04	0.26	0.23	0.18	0.48	0.32	1.27	0.86	0.08	0.07	0.08

Table 4. Correlation matrix for the experimental results (bold indicates coefficients ≥ 0.5).

	Max. Force	Fracture force	Stiff-ness	Disp. at Max. Force	% Disp. at Fracture	S_1	S_2	S_3	S_4	S_5	S_6	R_1	R_2	T_1	T_2	T_3	age
Max. Force	1.00																
Fracture force	**0.79**	1.00															
Stiffness	**0.75**	**0.59**	1.00														
Disp. Max. Force	0.26	0.32	-0.03	1.00													
Disp. at Fracture	-0.31	**-0.64**	-0.25	0.23	1.00												
S_1	0.43	0.47	0.00	0.42	-0.34	1.00											
S_2	0.26	0.33	0.09	0.47	0.08	**0.50**	1.00										
S_3	0.48	**0.54**	0.46	0.39	-0.05	0.14	0.38	1.00									
S_4	**0.50**	**0.67**	**0.52**	0.27	-0.17	0.06	**0.56**	**0.65**	1.00								
S_5	0.19	0.43	-0.04	**0.51**	-0.13	0.47	0.19	**0.59**	0.24	1.00							
S_6	0.28	0.11	0.08	0.06	-0.21	**0.60**	-0.15	-0.07	-0.32	0.12	1.00						
R_1	0.14	0.05	-0.02	0.01	-0.19	0.48	**0.50**	-0.43	-0.06	-0.41	0.22	1.00					
R_2	0.00	0.09	-0.13	0.07	0.13	0.31	**0.73**	0.00	0.48	-0.08	-0.20	**0.50**	1.00				
T_1	0.36	0.48	0.24	0.22	-0.29	**0.63**	0.10	0.31	0.03	**0.70**	0.41	-0.10	-0.19	1.00			
T_2	0.17	0.39	0.00	0.32	-0.37	0.48	-0.05	0.09	-0.20	**0.58**	0.21	-0.11	-0.35	**0.83**	1.00		
T_3	0.09	-0.01	0.21	-0.37	-0.19	0.11	-0.23	-0.32	-0.46	-0.19	0.10	0.16	-0.30	0.44	**0.56**	1.00	
age	**0.51**	**0.70**	0.24	0.48	**-0.53**	**0.64**	0.38	0.24	0.41	0.41	0.11	0.18	0.23	0.38	0.40	0.01	1.00

In summary, then, the parameter having the largest effect on the FE-calculated peak force and fracture displacement was the threshold used to define the cortical bone (see Table 5). Maximum stress in the elastic-plastic material model was also important, with a 35% change in Young's modulus having a relatively small effect. The element types and size ranges considered here had smaller effects.

Table 5. Peak forces obtained in the simulation of the different models.

Subject	M1	M2	M3	M4	M5	M6	M7	M8	M9	M10	Avg.
ECIP 01	3507	4773	2934	3086	2271	3247	2202	3713	2719	2299	3075.1
ECIP 03	4013	3870	4279	4292	4035	3766	3690	4611	4094	3272	3992.2
ECIP 04	3239	3186	3564	3651	1546	3702	3641	3877	3495	2858	3275.9
ECIP 05	3022	2987	1789	1783	2733	4274	1859	2400	1684	1394	2392.5
ECIP 06	4658	4409	4211	4218	4036	5072	3947	4259	3995	3312	4211.7
ECIP 07	3470	3633	3641	3926	3109	4034	3641	3507	3425	2960	3534.6
ECIP 08	3291	3496	5153	5280	3038	3983	4660	5479	4971	4058	4340.9
ECIP 09	2342	2388	3412	3452	2121	2859	3115	3562	3265	2691	2920.7
ECIP 10	3504	3390	4498	4535	3192	3997	4218	4677	4402	3563	3997.6
ECIP 11	2701	2691	3432	3506	2354	3154	3227	3610	3120	2673	3046.8
ECIP 12	3762	3811	4750	4946	3467	2094	4201	4859	4680	3720	4029.0
ECIP 13	2702	2646	3458	3490	2564	3033	3224	3705	3309	2754	3088.5
ECIP 14	2300	2263	3250	3041	3558	2594	2857	3186	2973	2504	2852.6
ECIP 15	4239	4526	5571	5752	4574	4732	4830	5395	5374	4347	4934.0
Mean	3339.3	3433.5	3853.0	3925.6	3042.7	3610.1	3522.3	4060.0	3679.0	3028.9	
Mean (norm. to M3)	0.867	0.891	1.000	1.019	0.790	0.937	0.914	1.054	0.955	0.786	

Table 6. Normalized (to M3) displacements at failure in the simulations (mean of all clavicles).

Subject	M1	M2	M3	M4	M5	M6	M7	M8	M9	M10
Mean (norm. to M3)	0.944	0.978	1.000	1.040	0.879	0.980	1.021	1.051	1.160	0.907

Table 7. Wilcoxon matched paired test.Comparison of the force (*) and displacement (◊) in the simulation models.

	M1	M2	M3	M4	M5	M6	M7	M8	M9	M10
M1										
M2	*/◊									
M3	**/◊◊	*/◊								
M4	**/◊◊	*/◊◊	**/◊							
M5	*/◊◊	**/◊◊	**/◊◊	**/◊◊						
M6	**/◊	*/◊	*/◊	*/◊◊	*/◊◊					
M7	*/◊◊	*/◊	**/◊	**/◊	*/◊◊	*/◊				
M8	**/◊◊	**/◊◊	**/◊	*/◊	**/◊◊	*/◊◊	**/◊			
M9	*/◊◊	*/◊◊	**/◊◊	**/◊◊	**/◊◊	*/◊◊	*/◊◊	**/◊◊		
M10	*/◊	*/◊◊	**/◊◊	**/◊◊	*/◊	**/◊◊	**/◊◊	**/◊◊	**/◊◊	

(*,◊= no statistical significant difference; **,◊◊=statistical significant difference, (p=0.05))

DISCUSSION

The FE sensitivity study revealed that the assumptions made during model development, even within a range that could be considered reasonable, can have significant effects on the prediction of fracture. In particular, the threshold used to differentiate cortical from trabecular bone and to define the periosteal and endosteal surfaces of the cortical shell bone a significant influence on the structural and failure mechanics. Future work should focus on the development of standards for thresholding biological materials from medical images. The FE simulations performed here were intended only to assess the sensitivity of various outcomes to a range of simulation parameters, and thus are not useful for identifying the most appropriate thresholding method or for establishing guidelines for future model development. Furthermore, no attempt was made to tune to model parameters to match the experimental results. Rather, a nominal modulus and material model were defined and the tested clavicles were used only to provide a range of reasonable geometries for consideration. A reasonable extension of the current work would be a more focused study on the modeling strategies that would result in the most accurate prediction of the experimental results.

Surprisingly, the elastic modulus, element type, and element size did not have large influences on the structural mechanics of the model. This likely reflects the fact that these parameters were not varied over a large range. The range studied was, however, within the range that is employed in current whole-body FE models, and which may be expected to be used in near-term future models. The results do, however, indicate that future model developers should pay particular attention to the mesh coarseness and to the tradeoff between computational efficiency and model performance.

The presence of trabecular bone on the FE model did not significantly affect any of the structural or failure mechanics. This seems reasonable since, first, the shape of the clavicle is such that the predominant loading mode is bending even under axial compression, and the stress distribution under bending is such that the magnitude of stress increases from the centroid to the outer layer of the structure. Second, the modulus of the cortical bone is significantly greater than the modulus of the trabecular core, so the cortical bone generates much larger stress for a given magnitude of strain and thus generates most of the internal force reacting against the applied moment.

Other interesting key finding of this study is that the age of the donor is a significant indicator of the force and displacement required to fracture the clavicle under axial loading. The 14-year-old subject's clavicle fractured after only 624 N of load, and the older subjects required significantly greater force and significantly less displacement to initiate fracture. This likely reflects the changes in bone material properties that occur between the ages of 14 and 56. Kemper et al. (2005) showed substantially lower modulus and greater failure strain for rib cortical bone harvested from an 18-year-old compared to bone from subjects in their 60s. The dimension S_4, which can be described as the diameter of the clavicle at the mid-span, was significantly related to fracture force and the pre-fracture stiffness, but other geometric factors, including the radii of the medial and lateral curvatures, were not significantly related to the structural behavior of this sample of clavicles. This illustrates that a variety of factors, including the properties over a range of length scales, influence the behavior of the clavicle under load. The age of the donors presented in this study is 44.6±12.7; there is a big difference with the previous research reported in the bibliography 76 ±12 (Duprey, 2007).

The analysis presented here supports our assertion in the Introduction that a large number of factors contribute to the outputs generated by an FE bone model developed from medical images. In fact, any FE model developed in this fashion will have so many independent parameters affecting the output that no set can be said to be uniquely "correct". In other words, relative to the experimental data typically available for benchmarking, the model parameters will be grossly under-determined. This fact calls into question the typical practice of "validating" a model by tuning selected parameters (usually material model coefficients) such that a set of experimental data are reproduced to some level of precision. In fact, the term "validation" is not appropriate when used to describe the type of whole-model composite assessment typically done in the field of injury biomechanics. It is more important that the mechanics of a model are correct than it is that the model matches some set of high-level experimental data that reflects many different aspects of the model without uniquely "validating" any single aspect.

ACKNOWLEDGEMENTS

We are thankful to Víctor Quintana for his assistance in the modeling of the clavicle images and to Dr. Sebastian Cruz for his collaboration harvesting the specimens. We also acknowledge the Depts. of Orthopedic Surgery and Anatomy and Forensic Medicine at CUN. Dr. Dámaso Aquerreta and the team of the Dept. of Imagery at CUN and Dr Ortiz de Solozano at CIMA assisted us in the processing of the images. Dr. Garcimartín and Dr. Maza and graduate student Martín at the Dept. of Physics. The work presented here has been partially supported by the University of Navarra faculty development PIUNA program (2007-04) and La Caixa (Obra Social).We would like also to thank Professors José María Bastero, Pilar Civeira, and Maria Seguí-Gómez for their support.

REFERENCES

Andermahr, J., Jubel, A., Elsner, A., Johann, J., Prokop, A., Rehm, K., Koebke, J. (2007) Anatomy of the clavicle and the intermedullary nailing of midclavicular fractures. Clinical Anatomy 20:48–56.
Boyd, S., Muller, R. (2005) Smooth surface meshing for automated finite element model generation from 3D data. J. Biomech. 39(7):1287-95.

Camacho, D., Hopper, R., Lin, G., Myers, B. (1997) An improved method for finite element mesh generation of geometrically complex structures with application to the skullbase. J. Biomech. 30(10):1067-70.

Charpail, E., Trosseille, X., Petit, P., Laporte, S., Lavaste, F., Vallancien, G. (2005) Characterization of PMHS ribs: a new test methodology. Stapp Car Crash Journal 49:1-16.

Charpail, E. (2006) Analyse du comportement mécanique des côtes en dynamique. Ph.D. dissertation released by the Ecole Nationale Supérieure d'Arts et Métiers (ENSAM), Paris.

Compigne, S., Caire, Y., Quesnel, T., and Verriest, J-P. (2004) Non-injurious and injurious impact response of the human shoulder - Three dimensional analysis of kinematics and determination of injury threshold. Stapp Car Crash Journal 48:89-125.

Duprey, S. (2007) Modélisation en elements finis du complexe de l'épaule et simulation de sa réponse à un choc latéral. Dissertation. Institut national des sciences appliquées de Lyon. France.

Duprey S., Bruyère K., Verriest J.P., Influence of Geometrical Personalization on the Simulation of Clavicle Fractures, Journal of Biomechanics (2008), vol.41(1), pp.200-207.

Ford, C., Keaveny, T., Hayes, W. (1996) The effect of impact direction on the structural capacity of the proximal femur during falls. J. Bone and Mineral Res. 11:377-83.

Iwamoto, M., Miki, K., Tanaka, E. (2005) Ankle skeletal injury predictions using anisotropic inelastic constitutive model of cortical bone taking into account damage evolution. Stapp Car Crash Journal 49:133-56.

Kemper, A., McNally, C., Kennedy, E., Manoogian, S., Rath, A., Ng, T., Stitzel, J., Smith, E., Duma, S. (2005) Material properties of human rib cortical bone from dynamic tension coupon testing. Stapp Car Crash Journal 49:199-230.

Keyak, J., Rossi, S., Jones, K., Skinner, H. (1998) Prediction of femoral fracture load using automated finite element modeling. J. Biomech. 31:125-33.

Keyak, J., Rossi, S. (2000) Prediction of femoral fracture load using finite element models: an examination of stress- and strain-based failure theories. J. Biomech. 33:209-14.

Kimpara, H., Lee, J., Yang, K.., King, A., Iwamoto, M., Watanabe, I., Miki, K. (2005) Development of a three-dimensional finite element chest model for the 5th percentile female. Stapp Car Crash Journal 49:251-69.

Ladd, A., Kinney, J. (1998) Numerical errors and uncertainties in finite-element modeling of trabecular bone. J. Biomech. 31(10):941-5.

Lee, S., Kent, R. (2007) Blood flow and fluid-structure interactions in the human aorta during traumatic rupture conditions. Stapp Car Crash Journal 51:211-233.

Lotz, J., Cheal, E., Hayes, W. (1991a) Fracture prediction for the proximal femur using finite element models: Part I – linear analysis. J. Biomech. Eng. 113:353-60.

Lotz, J., Cheal, E., Hayes, W. (1991b) Fracture prediction for the proximal femur using finite element models: Part II – Nonlinear analysis. J. Biomech. Eng. 113:361-5.

Nalla, R., Stolken, J., Kinney, J., Ritchie, R. (2005a) Fracture in human cortical bone: local fracture criteria and toughening mechanisms. J. Biomech. 38:1517-25.

Nalla, R., Kinney, J., Ritchie, R. (2005b) Effect of orientation on the in vitro fracture toughness of dentin: the role of toughening mechanisms. Biomat. 24:3955-68.

Pettersen, S., Nesje, L., Skallerud, B. (2006) The influence of CT parameters on Hounsfield units in cortical bone. J. Biomech. 39(Suppl 1):S6.

Ruan, J., El-Jawahri, R., Chai, L, Barbat, S., Prasad, P. (2003) Prediction and analysis of human thoracic impact responses and injuries in cadaver impacts using a full human body finite element model. Stapp Car Crash Journal 47:299-321.

Ruan, J., El-Jawahri, R., Rouhana, S., Barbat, S., Prasad, P. (2006) Analysis and evaluation of the biofidelity of the human body finite element model in lateral impact simulations according to ISO-TR9790 procedures. Stapp Car Crash Journal 50:491-507.